Color separation of high-density dielectric rectangular grating in the Fresnel diffraction region

Yue Fang, Qiaofeng Tan,* Mingqian Zhang, and Guofan Jin

State Key Laboratory of Precision Measurement Technology and Instruments, Tsinghua University, Beijing 100084, China

*Corresponding author: tanqf@mail.tsinghua.edu.cn

Received 3 January 2012; accepted 28 February 2012;
posted 6 March 2012 (Doc. ID 160641); published 20 April 2012

A high-density dielectric rectangular grating is designed for color separation in a Fresnel diffraction field. The Fresnel field distribution is analyzed and the optimization conditions for color separation are given. The process of the modes propagating and energy exchanging with the diffraction orders are expressed by modal method. The color separation for different polarizations can be realized. The energy efficiency is 96.3% at the 633 nm wavelength and 86.9% at the 488 mm wavelength for both TE polarizations, while the energy efficiency is theoretically 96.3% at the 633 nm wavelength for TE polarization and 90.6% at the 488 nm wavelength for TM polarization. The field distributions are scanned by the near-field scanning optical microscopy, and the efficiency is 71.2% for the 633 nm wavelength and 67.3% for the 488 nm wavelength for both TE polarizations experimentally.

OCIS codes: 050.1950, 050.6624, 230.1950.

1. Introduction

The dielectric rectangular grating, as one of the most basic optical components, has a very wide range of applications. Now the fabrication technology allows a smaller grating etching so this kind of high-density rectangular grating shows a lot of novel and interesting features [1–4]. The modal method first presented by Botten [5] is used to analyze and design a rectangular grating by many researchers as a simplified method. A. V. Tishchenko provided a phenomenological modal representation of deep and high contrast lamellar gratings [6]. Clausnitzer *et al.* explained the high-efficient and polarization-dependent effect of rectangular transmission gratings [7,8]. Feng *et al.* and Cao *et al.* designed the beam splitter and polarizing beam splitter grating by means of this method [9,10]. Also, other kinds of gratings, such as the triangle, the sinusoidal-groove, and the double-groove, can be designed by this method [11,12].

With near-field scanning optical microscopy (NSOM) widely used in scientific studies, the researchers have revealed a number of interesting phenomena in the near field of various kinds of nanostructures. Recently, the field distributions in the Fresnel field, which are often a few microns away from the objects, have received more concern. The apparent superresolution of periodic grating optical imaging was found in this region [13]. Moreover, the Talbot effect, which is the well-known scalar diffraction Fresnel field optical phenomenon, was also found in this region, but in different Talbot distance and distribution forms. Lu *et al.* presented the polarization-dependent Talbot effect both theoretically and experimentally [14]. Teng discussed the quasi-Talbot effect for both scalar grating and high-density grating [15,16]. These effects show promise for many practical applications such as microlithography, information storage, and optical imaging.

In this paper, we report a novel function of high-density dielectric rectangular grating, i.e., color-separation grating in the Fresnel diffraction region, which has been verified by experiments. To the best of our knowledge, we are the first to use such

1559-128X/12/122172-06$15.00/0

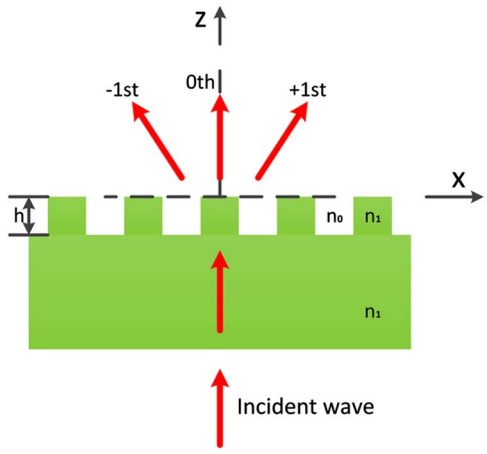

Fig. 1. (Color online) Schematic of the grating.

a grating to realize a novel function. The color-separation gratings are often used to separate incident lights with different wavelengths, but in this paper we separate the distributions of different wavelengths in the Fresnel diffraction region. We discuss the Fresnel field of the dielectric rectangular grating and give the optimization objectives for color separation in Section 2. According to the modal method, the mode propagating explanation is presented to analyze the grating problem, and the calculation is conducted in Section 3. The experimental results are shown in Section 4. Section 5 is the conclusion of this paper.

2. Grating Design

The rectangular grating we discussed and fabricated is shown in Fig. 1. The period of the grating is 1.5λ ($\lambda =$ the 633 nm wavelength), and the duty cycle is 0.5. The monochromatic plane wave normally illuminates from the substrate side. The polarization of the incident wave is the TE mode, where the electric field is perpendicular to the incident plane. According to the Sellmeier equation, the refractive indices of fused silica at different wavelengths in the visible light region are in the range from 1.45 to 1.47 [17]. The dispersion has little effect on the design, so the refractive index of the fused-silica grating layer and the substrate are chosen as 1.45 for the calculations hereafter.

Figure 2 shows the calculated diffraction distributions of the grating with different incident wavelengths along the z axis. We can see that the distribution is sensitive to the wavelength and at a certain distance, the distribution of the diffraction field repeats itself, which is called the quasi-Talbot effect in the Fresnel region. Besides the periodicity of the field along the propagating direction, the fields with different wavelengths have different distributions. This means that it is possible the peaks of intensity of different incident lights show alternately. That is to say, the grating can realize color separation.

We define the plane from the grating surface where the diffraction fields of different wavelengths can separate with each other the color-separation plane. Therefore, the depth of the grating and the color-separation plane are the optimization parameters that we need to determine. The diffraction field of the grating is the interference of diffracted orders and the intensity distribution can be written as

$$\begin{aligned} I &= E_{\text{tot}} \times E_{\text{tot}}^{*} \\ &= E_0^2 + 4E_0E_{+1}\cos[(\beta_0 - \beta_{+1})z \\ &\quad + (\varphi_0 - \varphi_{+1})]\cos(Kx) + 4E_{+1}^2\cos^2(Kx), \end{aligned} \tag{1}$$

where E_0 and E_{+1} are the amplitudes of the zeroth and first diffraction orders, respectively; ϕ_0 and ϕ_{+1} are the phases of the zeroth and first diffraction orders, respectively; β_0 and β_{+1} are the propagating constants of the zeroth and first diffraction orders, respectively; and K is the grating vector. We will design a grating that can separate two incident waves with wavelengths 633 and 488 nm. First, we should optimize the depth of the grating to focus more energy within half of the grating period, which

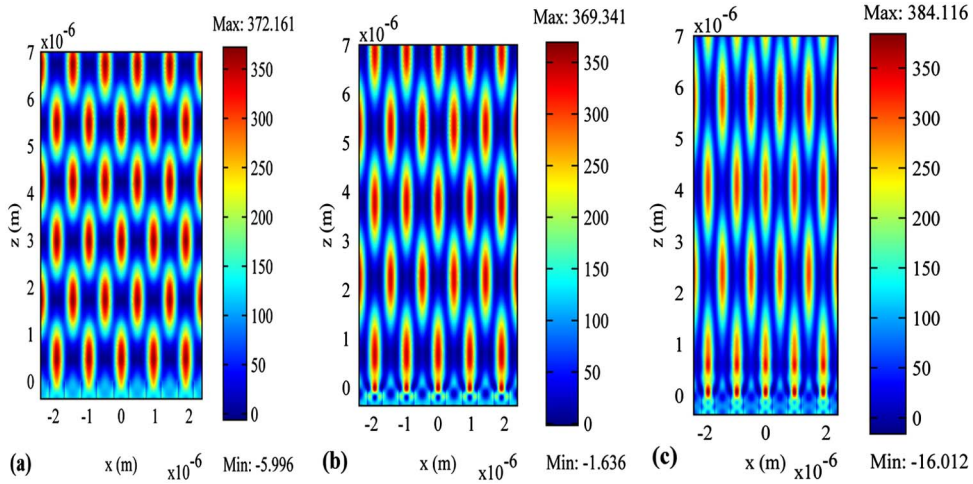

Fig. 2. (Color online) Diffraction distributions of different incident lights for (a) 633 nm, (b) 532 nm, and (c) 488 nm.

maximizes the integral of the intensity distribution in half of the grating period, and can be equivalently written as a mathematical expression:

$$\max \int_{x_{\max}-\frac{d}{4}}^{x_{\max}+\frac{d}{4}} I \mathrm{d}x, \tag{2}$$

where d is the period of the grating. By solving the optimization objective function in Eq. (2), we can get the amplitude optimization condition,

$$E_0 = \sqrt{2} E_{+1}. \tag{3}$$

where $k_x = k_0 n_1 \sin\theta$; $k_1 = k_0(n_1^2 - n_{\text{eff}}^2)^{1/2}$; $k_2 = k_0(n_0^2 - n_{\text{eff}}^2)^{1/2}$; d is the period of the grating; λ is the wavelength of the incident wave; θ is the angle of the incident wave; and $n_{\text{eff}} = \beta_{\text{eff}}/k_0$ is the effective index of the grating mode. In the case of normal incidence, the right side is equal to 1. The grating modes with $n_{\text{eff}} > 0$ are propagating, so with this condition we can solve the transcendental Eq. (5). Three modes solutions are obtained, and the effective indices of the grating modes are $n_{\text{eff}0} = 1.4222$, $n_{\text{eff}1} = 1.1729$, and $n_{\text{eff}2} = 0.9278$, respectively. The TE mode field can be given analytically as [18]

$$\phi_e = \begin{cases} \cos(k_1 x) & 0 \le |x| \le fd/2 \\ \cos(k_1 fd/2)\cos[k_2(|x| - fd/2)] - \frac{k_1}{k_2}\sin(k_1 fd/2)\sin[k_2(|x| - fd/2)] & fd/2 \le |x| \le d/2 \end{cases}, \tag{6}$$

$$\phi_e = \begin{cases} \frac{1}{k_1}\sin(k_1 x) & 0 \le |x| \le fd/2 \\ \frac{1}{k_1}\,\mathrm{sgn}(x)\{\sin(k_1 x/2)\cos[k_2(|x| - fd/2)] + \frac{k_1}{k_2}\cos(k_1 fd/2)\sin[k_2(|x| - fd/2)] & fd/2 \le |x| \le d/2 \end{cases}. \tag{7}$$

The amplitude is a function of the depth of the grating, so the depth is determined by Eq. (3), which will be discussed in detail in Section 3. Also, the phase distribution between different wavelengths should be matched by Eq. (4):

$$\begin{cases} (\beta_{r0} - \beta_{r1})z + (\phi_{r0} - \phi_{r1}) = 2\,m\pi, & m \in \text{integral} \\ (\beta_{b0} - \beta_{b1})z + (\phi_{b0} - \phi_{b1}) = \left(n + \frac{1}{2}\right)\pi, & n \in \text{integral} \end{cases}, \tag{4}$$

where ϕ_{ri} and ϕ_{bi} are the phases of the ith diffraction order with different incident lights; β_{ri} and β_{bi} are the phases of the ith diffraction order with different incident lights ($i = -1, 0, +1$).

3. Modal Method

Other than rigorous coupled wave analysis (RCWA), the modal method expands the electromagnetic field in the grating region in terms of true propagating modes. The propagating constants of the grating modes can be determined by the characteristic equation for TE [5]:

$$\begin{aligned} F(n_{\text{eff}}^2) &= \cos(k_1 fd)\cos(k_2(1-f)d) \\ &\quad - \frac{k_1^2 + k_2^2}{2k_1 k_2}\sin(k_1 fd)\sin(k_2(1-f)d) \\ &= \cos(k_{x,\text{inc}} d), \end{aligned} \tag{5}$$

It is explicit that φ_e represents the even mode and φ_0 represents the odd mode of the grating. The energy exchanged between the incident wave and the modes can be calculated by the overlap integral [8]:

$$t_q = \frac{\left|\int E_{yn}(x,0)\cdot\varphi_m(x)\mathrm{d}x\right|^2}{\int |E_{yn}(x,0)|^2 \mathrm{d}x \cdot \int |\varphi_m(x)|^2 \mathrm{d}x}. \tag{8}$$

Only the even mode can be excited because the integral of the odd function in a period is zero. The profiles of the first two even modes are shown in Fig. 3. In this paper, we only consider the two propagating modes, and the high evanescent modes are neglected.

According to the modal method, the modes excited by incident light will propagate through the grating region and transform to the diffraction orders. The energy exchanged between the modes and the diffraction orders can also be obtained by Eq. (8). The field at the air-grating interface can be expressed as

$$\begin{aligned} &t_0\varphi_0(x)\exp(-ik_z n_{\text{eff}0} h) + t_2\varphi_2(x)\exp(-ik_z n_{\text{eff}2} h) \\ &\quad = E_1 e^{-ik_{x,\text{dif}}x} + E_0 + E_{-1} e^{ik_{x,\text{dif}}x}, \end{aligned} \tag{9}$$

where t_0 is the transmission coefficient of the zeroth mode and t_1 is the transmission coefficient of the first mode. Together with the amplitude condition in Eq. (3), the depth of the grating can be decided, and the optimal depth is 0.3795 μm. The result is coincident with the depth calculated by RCWA,

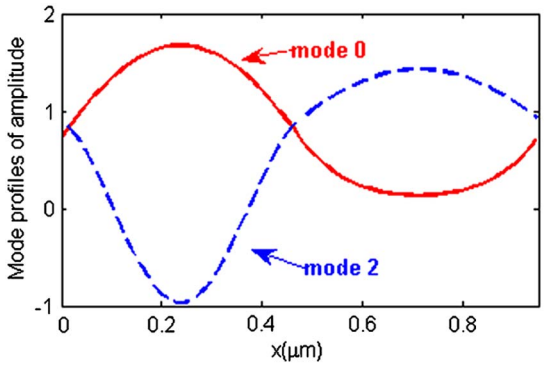

Fig. 3. (Color online) The profile of the grating modes.

which is 0.374 μm. By solving the phase-matching condition in Eq. (4), the color-separation plane is obtained at $z = 4.2$ μm. The intensity distributions of the two incident lights with wavelengths at 633 nm and 488 nm at plane $z = 4.2$ μm is shown in Fig. 4. The energy efficiency for each incident light is defined as the integral of intensity in half of the period divided by the integral of intensity in one period, so the energy efficiency is 96.3% for the 633 nm wavelength and 86.9% for the 488 nm wavelength.

The method is also suitable for TM polarization, where the magnetic field is perpendicular to the incident plane, so the color separation for different polarizations can also be realized. We will design a color-separation grating at the 633 nm wavelength for TE polarization and at the 488 nm wavelength for TM polarization as an example. The characteristic equation for TM polarization is [5]

$$\begin{aligned} F(n_{\text{eff}}^2) &= \cos(k_1 f d)\cos(k_2(1-f)d) \\ &\quad - \frac{\varepsilon_1^2 k_1^2 + \varepsilon_2^2 k_2^2}{2\varepsilon_1\varepsilon_2 k_1 k_2}\sin(k_1 f d)\sin(k_2(1-f)d) \\ &= \cos(k_{x,\text{inc}} d). \end{aligned} \tag{10}$$

The first two propagating even modes at the 488 nm wavelength are 1.4653 and 1.0569. Using the phase matching condition [Eq. (4)], we can still get the color-separation plane at $z = 4.2$ μm because the phase difference between the zeroth order and the first order for TE polarization and TM polarization are small at the 488 nm wavelength. The intensity distribution is shown in Fig. 5, and the energy efficiency is 96.3% at the 633 nm wavelength for TE polarization and 90.6% at the 488 nm wavelength for TM polarization.

4. Experimental Results

The grating was fabricated by electron-beam direct-writing lithography. The experimental setup is shown in Fig. 6(a). The He–Ne laser with the 633 nm wavelength and the semiconductor laser with the 488 nm wavelength are used as the incident light sources. The polarization beam splitter is the beam combiner to ensure that the two different incident lights can illuminate at the same position of the grating. The grating was placed on the sample stage, which is shown in Fig. 6(b). The Fresnel field distribution above the grating is scanned using NSOM, which is a product of the NT-MDT Company. The NSOM can realize a two-dimensional scan and the positioning accuracy is in the order of 10 nm.

We chose an area with a better profile at the size of 10 μm × 10 μm, and the near-field grating profile scanning result is shown in Fig. 7(a). The width of the grating has been broadened due to the convolution effects of the shape of the fiber probe tip. The grating was illuminated by two incident lights, and Figs. 7(b) and 7(c) show the field distributions with wavelengths at 633 nm and 488 nm, respectively. Figure 7(d) is a cross section at the same position from Figs. 7(b) and 7(c). The averaged energy efficiencies are 71.2% and 67.3% for wavelengths at 633 nm and 488 nm, respectively. The intensity distribution difference between the two incident lights is to a large extent due to the input power differences between the two laser sources, but this factor does not affect the efficiency calculations. As we can see, the experimental result is consistent with the simulated result shown in Fig. 4. However, the uniformity of intensity distribution and the distribution at the 488 nm wavelength are not as good as the

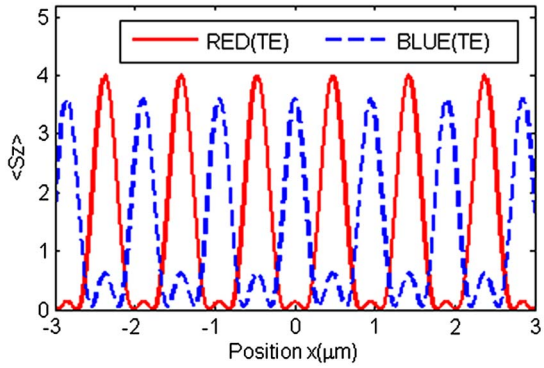

Fig. 4. (Color online) Intensity distribution of the two incident lights with the 633 nm and 488 nm wavelengths at plane $z = 4.2$ μm.

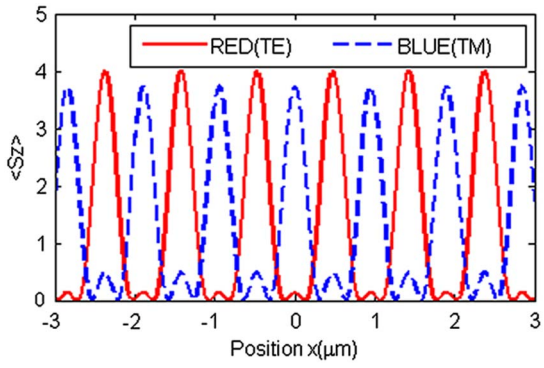

Fig. 5. (Color online) Intensity distribution of the two incident lights with the 633 nm wavelength for TE polarization and 488 nm for TM polarization at plane $z = 4.2$ μm.

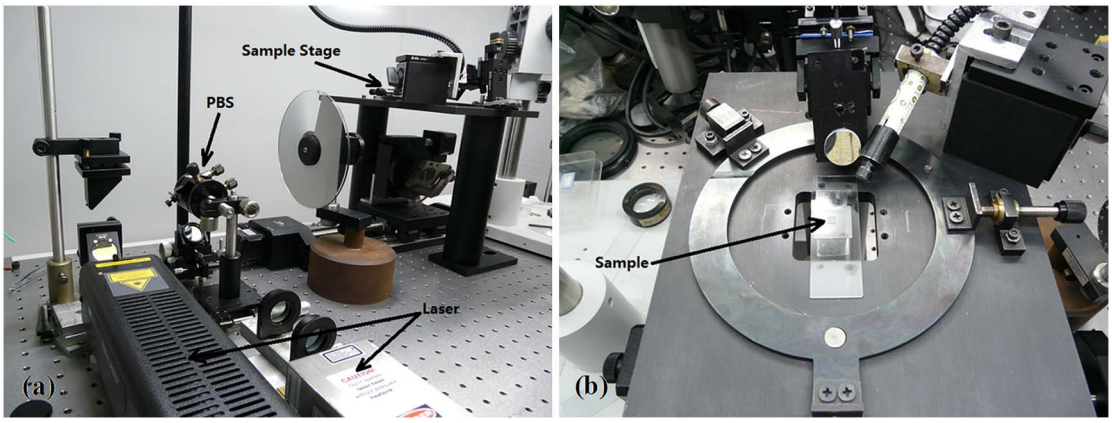

Fig. 6. (Color online) The configuration of the (a) experimental setup and (b) sample stage.

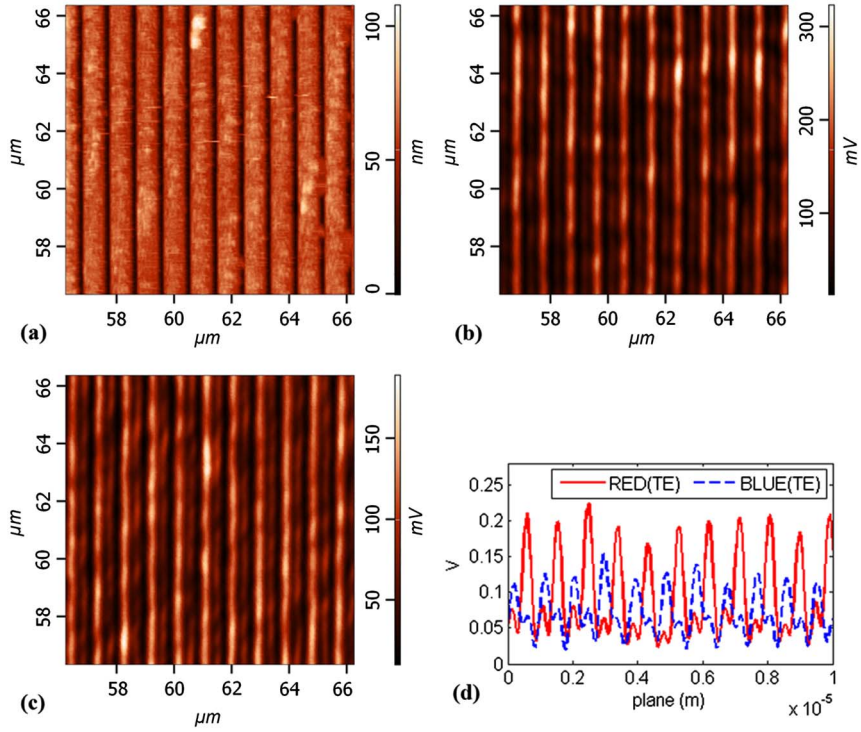

Fig. 7. (Color online) Experimental results scanned by NSOM at $z = 4.2$ μm: (a) the near-field grating profile scanning, (b) the field distribution with the wavelength at 633 nm, (c) the field distribution with the wavelength at 488 nm, and (d) the intensity distribution at the same cross section from 7(b) and 7(c).

simulation result. On the one hand, this is because the fiber tip has been used so many times that the quality of the results decline gradually. On the other hand, we will further optimize the grating structure to obtain a better result.

5. Conclusion

We analyze the field distribution of the dielectric rectangular grating in the Fresnel region and give the amplitude optimization condition and the phase matching condition. A color-separation grating is designed for the 633 and 488 nm wavelengths for different polarizations using the analytical solution of the modal method, which can give a physical explanation of the modes' propagating process in the grating region. Theoretically, the energy efficiency is 96.3% for the 633 nm wavelength and 86.9% for the 488 nm wavelength for both TE polarizations, and the energy efficiency is 96.3% at the 633 nm wavelength for TE polarization and 90.6% at the 488 nm wavelength for TM polarization. The color separation is observed at the plane $z = 4.2$ μm with the use of NSOM. The energy efficiencies obtained by experiments are 71.2% and 67.3% at the 633 nm wavelength and 488 nm for both TE polarizations, respectively, which is consistent with the simulation results.

This work was supported by the National Natural Science Foundation of China (60978047, 60678033) and National Basic Research Program of China (2007CB935303). The experiment was completed in the Nano Optics Laboratory directed by Prof. Jia Wang at Tsinghua University.

References

1. D. Delbeke, R. Baets, and P. Muys, "Polarization-selective beam splitter based on a highly efficient simple binary diffraction grating," Appl. Opt. **43**, 6157–6165 (2004).
2. A. Drauschke, "Analysis of nearly depth-independent transmission of lamellar gratings in zeroth diffraction order in TM polarization," J. Opt. **8**, 511–517 (2006).
3. C. Tina, K. Thomas, B. Frank, H. Roland, K. Ernst-Bernhard, and T. Andreas, "Reflection-reduced encapsulated transmission grating," Opt. Lett. **33**, 1972–1974 (2008).
4. H. Rathgen and H. L. Offerhaus, "Large bandwidth, highly efficient optical gratings through high index materials," Opt. Express **17**, 4268–4283 (2009).
5. I. C. Botten, M. S. Craig, R. C. McPhedran, J. L. Adams, and J. R. Andrewartha, "The dielectric lamellar diffraction grating," Opt. Acta **28**, 413–428 (1981).
6. A. V. Tishchenko, "Phenomenological representation of deep and high contrast lamellar gratings by means of the modal method," Opt. Quantum Electron. **37**, 309–330 (2005).
7. T. Clausnitzer, T. Kämpfe, E.-B. Kley, A. Tünnermann, U. Peschel, A. V. Tishchenko, and O. Parriaux, "An intelligible explanation of highly-efficient diffraction in deep dielectric rectangular transmission gratings," Opt. Express **13**, 10448–10456 (2005).
8. T. Clausnitzer, T. Kämpfe, E.-B. Kley, A. Tünnermann, A. Tishchenko, and O. Parriaux, "Investigation of the polarization-dependent diffraction of deep dielectric rectangular gratings illuminated in Littrow mounting," Appl. Opt. **46**, 819–826 (2007).
9. J. Feng, C. Zhou, B. Wang, J. Zheng, W. Jia, H. Cao, and P. Lv, "Three-port beam splitter of a binary fused-silica grating," Appl. Opt. **47**, 6638–6643 (2008).
10. H. Cao, C. Zhou, J. Feng, P. Lu, and J. Ma, "Design and fabrication of a polarization-independent wideband transmission fused-silica grating," Appl. Opt. **49**, 4108–4112 (2010).
11. J. Feng, C. Zhou, H. Cao, and P. Lu, "Unified design of sinusoidal-groove fused-silica grating," Appl. Opt. **49**, 5697–5704 (2010).
12. J. Wu, C. Zhou, H. Cao, A. Hu, J. Yu, W. Sun, and W. Jia, "Beam splitting of a double-groove fused-silica grating under normal incidence," J. Opt. **13**, 115703 (2011).
13. I. I. Smolyaninov and C. C. Davis, "Apparent superresolution in near-field optical imaging of periodic gratings," Opt. Lett. **23**, 1346–1347 (1998).
14. Y. Lu, C. Zhou, S. Wang, and B. Wang, "Polarization-dependent Talbot effect," J. Opt. Soc. Am. A **23**, 2154–2160 (2006).
15. S. Teng, N. Zhang, Q. Dong, and C. Cheng, "Diffraction of a one-dimensional phase grating in the deep Fresnel field," J. Opt. Soc. Am. A **24**, 3636–3643 (2007).
16. S. Teng, Y. Tan, and C. Cheng, "Quasi-Talbot effect of the high-density grating in near field," J. Opt. Soc. Am. A **25**, 2945–2951 (2008).
17. B. Brixner, "Refractive-index interpolation for fused silica," J. Opt. Soc. Am. **57**, 674–676 (1967).
18. L. Li, "A modal analysis of lamellar diffraction gratings in conical mountings," J. Mod. Opt. **40**, 553–573 (1993).